A computational toolbox to investigate the metabolic potential and resource allocation in fission yeast

Pranas Grigaitis[1,#], Douwe A. J. Grundel[1,2], Eunice van Pelt-KleinJan[1,3], Mirushe Isaku[1], Guixiang Xie[1], Sebastian Mendoza Farias[1], Bas Teusink[1], and Johan H. van Heerden[1]

[1] Systems Biology Lab, Amsterdam Institute of Molecular and Life Sciences (AIMMS), Vrije Universiteit Amsterdam, De Boelelaan 1085, 1081HV Amsterdam, the Netherlands

[2] Present address: Molecular Systems Biology, Groningen Biomolecular Sciences and Biotechnology Institute, University of Groningen, Nijenborgh 4, 9747AG Groningen, the Netherlands

[3] TiFN, P.O. Box 557, 6700AN Wageningen, the Netherlands

Correspondence to P. Grigaitis: p.grigaitis@vu.nl or J. H. van Heerden: j.van.heerden@vu.nl

Abstract

The fission yeast *Schizosaccharomyces pombe* is a popular eukaryal model organism for cell division and cell cycle studies. With this extensive knowledge of its cell and molecular biology, *S. pombe* also holds promise for use in metabolism research and industrial applications. However, unlike the baker's yeast *Saccharomyces cerevisiae*, a major workhorse in these areas, cell physiology and metabolism of *S. pombe* remain less explored. One way to advance understanding of organism-specific metabolism is construction of computational models and their use for hypothesis testing. To this end, we leverage existing knowledge of *S. cerevisiae* to generate a manually-curated high-quality reconstruction of *S. pombe's* metabolic network, including a proteome-constrained version of the model. Using these models, we gain insights into the energy demands for growth, as well as ribosome kinetics in *S. pombe*. Furthermore, we predict proteome composition and identify growth-limiting constraints that determine optimal metabolic strategies under different glucose availability regimes, and reproduce experimentally determined metabolic profiles. Notably, we find similarities in metabolic and proteome predictions of *S. pombe* with *S. cerevisiae*, which indicate that similar cellular resource constraints operate to dictate metabolic organization. With these use cases, we show, on the one hand, how these models provide an efficient means to transfer metabolic knowledge from a well-studied to a lesser-studied organism, and on the other, how they can successfully be used to explore the metabolic behaviour and the role of resource allocation in driving different strategies in fission yeast.

Introduction

The fission yeast *Schizosaccharomyces pombe* is a popular eukaryal model organism for cell division and cell cycle studies. With this extensive knowledge of its cell and molecular biology, *S. pombe* also holds promise for use in metabolism research and industrial applications. However, unlike the baker's yeast *Saccharomyces cerevisiae*, a major workhorse in these areas, cell physiology and metabolism of *S. pombe* remain much less explored. While these two yeasts share some similarities, distinct differences in e.g. cell cycle regulation (Forsburg and Nurse, 1991), mode of cell division (Hoffman et al., 2015), glucose transport (Hofer and Nassar, 1987) and utilizable carbon sources (de Jong-Gubbels et al., 1996) makes *S. pombe* a highly complementary model for studies into eukaryotic metabolism. A deeper understanding of *S. pombe* metabolism, therefore, offers opportunities to expand our knowledge of the larger eukaryal metabolic landscape. In this regard, computational approaches can provide a useful means to leverage the extensive metabolic knowledge from *S. cerevisiae* to explore *S. pombe* metabolism.

Computational approaches have become increasingly important to unravel and understand metabolism in diverse species, ranging from bacteria to humans. Arguably the most successful approaches in both applied and fundamental research are based on Genome-scale metabolic models (GEMs) (Fang et al., 2020). A GEM is a computable knowledge-base which is essentially a compendium of all reactions of an organism: its metabolic potential, based on the genome sequence. GEMs have successfully been applied in diverse settings, including the metabolic engineering of microorganisms (McAnulty et al., 2012; Mishra et al., 2018), studies of human diseases or disease causing pathogens (Beste et al., 2007; Branco dos Santos et al., 2017), drug development (Kim et al., 2011), and the investigation of interactions within microbial communities (Dukovski et al., 2021). Furthermore, by providing a general framework based on the genome sequence of an organism, GEMs allow for efficient transfer of metabolic knowledge between organisms.

GEMs of *S. pombe* have previously been constructed. However, several issues, including incompatibility with current Systems Biology Markup Language (SBML) standards (Pitkänen et al., 2014; Sohn et al., 2012), a lack of gene-protein-reaction (GPR)-associations, or automated reconstruction without additional curation (Lu et al., 2021; Pitkänen et al., 2014), significantly limited their utility. Furthermore, recent extensions of the GEM framework to include regulation and resource allocation dynamics now enable the exploration of complex metabolic behaviours such as the Crabtree-effect (analogous to the Warburg-effect seen in human cells) that cannot be explained with conventional GEMs.

Thus in this study, we exploited the extensive metabolic knowledge and modelling toolset available for *S. cerevisiae* to generate an updated computational toolbox for *S. pombe*, consisting of a genome-scale metabolic model, *pomGEM*, and a resource allocation model, *pcPombe*. We manually curated and calibrated both models using published experimental data. We used the *pcPombe* model to identify proteome constraints that dictate the growth and metabolic strategy of *S. pombe* in glucose-limited chemostat cultures. We find that behaviour appears to be governed by constraints similar to those operating in *S. cerevisiae*. These models provide essential tools to further expand knowledge of *S. pombe's* metabolism, specifically, and eukaryotic metabolism in general.

Results

Reconstruction of the *S. pombe* metabolic network

We first aimed to create a manually-curated, high-quality reconstruction of the *S. pombe* metabolic network. Therefore, we coupled automated reconstruction tools (using *Saccharomyces cerevisiae* metabolic reconstruction *Yeast8.3.3* (Lu et al., 2019) as a template) with thorough manual curation (Methods) in order to construct the *pomGEM*, a manually-curated GEM of *S. pombe* (Figure 1a) that meets current standards for annotation and reusability. Manual curation of newly-reconstructed GEMs is critical

for accurate prediction of metabolic phenotypes. For example, during the curation we removed the reactions of glyoxylate cycle, a pathway that is active in *S. cerevisiae* but absent in *S. pombe* (de Jong-Gubbels et al., 1996), and the reason why *S. pombe* cannot utilize two-carbon compounds for growth. In addition, we replaced the biomass objective function (BOF) of the *Yeast8.3.3* model with the BOF, used in the SpoMBEL1693 model (Sohn et al., 2012), which is based on experimental measurements of *S. pombe* (Figure 1b).

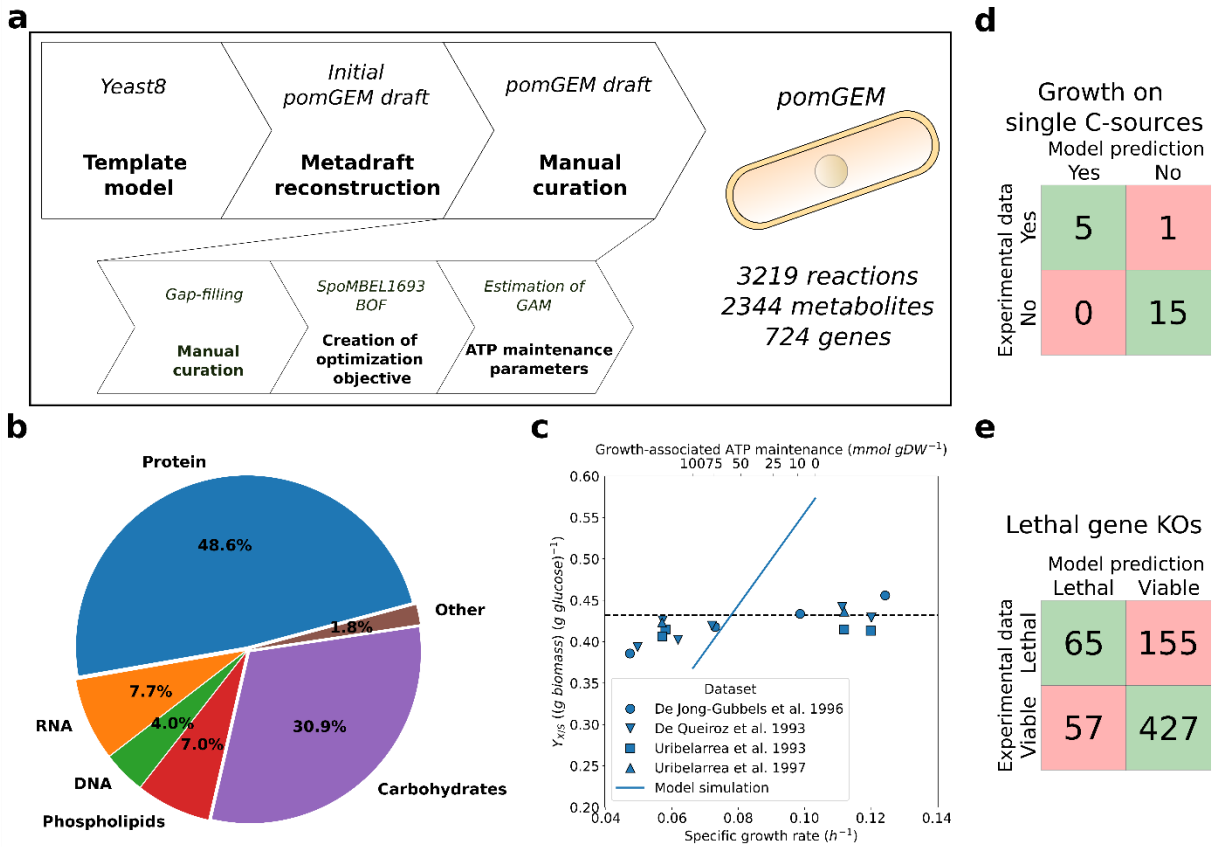

Figure 1. Reconstruction of the *pomGEM*, the genome-scale metabolic model of *S. pombe* **a**. The workflow of the reconstruction. **b.** The composition of *S. pombe* biomass, defined in the *pomGEM*. **c.** Estimation of the GAM value. Glucose uptake flux was fixed to 1.0 $mmol\ gDW^{-1}\ h^{-1}$ and the maximal specific growth rate μ was predicted with varying GAM value. Growth yield on glucose $Y_{X/S}$ was computed based on the predicted specific growth rate. The target yield on glucose ($Y_{X/S} = 0.432g\ biomass\ (g\ glucose)^{-1}$) was computed as an average of experimentally determined $Y_{X/S}$ from glucose-limited cultures with $D > 0.1h^{-1}$ (de Jong-Gubbels et al., 1996; de Queiroz et al., 1993; Uribelarrea et al., 1997, 1993). **d-e.** Benchmarking of the *pomGEM* model: **d.** Prediction of growth on single carbon sources (experimental data from (Choi et al., 2010) and our measurements, see Supplementary Table 1 for details); **e.** Prediction of the lethality of single gene KOs (experimental data from (Kim et al., 2010)). Abbreviations: BOF, biomass objective function; GAM, growth-associated maintenance; KO, knock-out.

Next, we looked at the energetic parameters. First, we confirmed that the P/O ratio (ATP produced per oxygen atom reduced) in the model is 1.28, consistent with experimental measurements (de Queiroz et al., 1993). In terms of ATP maintenance parameters, we kept the non-growth-associated ATP maintenance (NGAM) demand at $0.7\ mmol\ gDW^{-1}\ h^{-1}$ from the *Yeast8.3.3*, in agreement with experimentally determined values for *S. pombe* (0.66 - $0.83\ mmol\ gDW^{-1}\ h^{-1}$) (de Queiroz et al., 1993). Furthermore, we estimated the growth-associated ATP maintenance (GAM) value (Figure 1c). We used published experimental measurements of growth yield on glucose ($Y_{X/S}$) in fully-respiratory glucose-limited cultures of *S. pombe* and varied the GAM value to achieve the target yield $Y_{X/S} = 0.432\ g\ biomass\ (g\ glucose)^{-1}$. The target $Y_{X/S}$ corresponded to $GAM = 58.3\ mmol\ gDW^{-1}$, comparable with $55.3\ mmol\ gDW^{-1}$ in the *Yeast8.3.3*. The *pomGEM* model showed very good agreement for the predicted flux values in central carbon metabolism with measured fluxes in glucose-limited chemostat cultures at $D = 0.1h^{-1}$ (Klein et al., 2013) (Supplementary Figure 1) .

We benchmarked the *pomGEM* model by predicting growth on a panel of 21 single carbon sources (Figure 1d, Supplementary Table 1) and lethality of single-gene knock-outs (KOs, Figure 1e, Supplementary Table 2). Predictions of growth on single carbon sources were correct for all carbon sources except one, ribose: (Choi et al., 2010) reported growth on ribose but *pomGEM* predicted no growth (false negative). It should be noted that the growth medium used for testing in (Choi et al., 2010) is not clearly defined, as such it cannot be unambiguously concluded that this strain can grow on D-ribose as sole carbon source. Of the predicted phenotypes, 69.9% of single-gene KOs were true predictions (match between model and experimental data) for the entire dataset, while false positives (viable only *in silico*) and false negatives (viable only *in vivo*) were 22.0% and 8.1% of the dataset, respectively. We, however, were not able to test the single-gene KOs on previously published reconstructions due to inherent technical issues with these models.

We also performed a check on the reaction essentiality to compare the prediction accuracy with the *SpoMBEL1693* model, where essentiality as assessed in terms of reactions rather than genes. We determined the essentiality (Methods) of 2017 model reactions with gene-protein-reaction (GPRs) associations, and mapped the GPRs with the individual genes in the dataset of gene KOs (Supplementary Table 3). *pomGEM* showed a true prediction rate of 74.7%, a good improvement (13.5%) on the true prediction rate achieved by *SpoMBEL1693* reconstruction (61.2%, (Sohn et al., 2012)).

Development of the proteome-constrained model of *S. pombe*

FBA-based models are powerful tools to investigate the potential of metabolic networks, but the ground assumptions of the method limit the prediction of metabolic phenotypes. As a rule, FBA predictions will identify the metabolic strategy that leads to the highest biomass yield on the limiting nutrient. For instance, under glucose-limited conditions, a GEM of *S. cerevisiae* will always predict a high-yield ATP production strategy, complete respiration of glucose to CO_2 and water, therefore. In reality, cells will switch to fermentation, a lower ATP-yield strategy, beyond a critical concentration of glucose. Thus, metabolic phenotypes which do not correspond to the highest-yield strategy cannot be predicted with FBA, unless additional constraints are added that reflect physiological constraints (de Groot et al., 2020).

An important constraint relates to the allocation of limited cellular resources. If metabolic reaction-associated protein costs are accounted for, different condition-dependent modes of growth, e.g. the switch between respiration and fermentation (Chen and Nielsen, 2019) can be reproduced. GEMs therefore can be improved by introducing the concept of resource allocation: optimal partitioning of the limited resources among the metabolic processes, based on the costs of energy and biosynthetic

resources (e.g. amino acids) needed for implementing each metabolic pathway. Over the last 15 years, different extensions of GEMs were proposed in order to predict optimal resource allocation in different microorganisms (De Becker et al., 2022). Recently, we introduced a proteome-constrained (*pc*-) model of *S. cerevisiae* (*pcYeast*) (Elsemman et al., 2022) that can accurately predict low and high biomass yield strategies under different growth conditions. In a similar spirit, we constructed *pcPombe*, a proteome-constrained model of *S. pombe*, on the basis of the *pomGEM* model (Figure 2a).

The *pcPombe* model (model explained in detail in Supplementary Notes) captures the interplay of metabolism and cellular resource allocation by (i) coupling metabolic processes with respective protein demand, and (ii) coupling protein abundance with compartment-specific proteome capacity constraints. We thus first extended the metabolic model by introducing fine-grained descriptions of protein turnover (reactions protein synthesis, folding, degradation, and dilution by growth). Then, we compiled data from literature and/or specialized biological databases (Methods, Supplementary Notes) to parametrize the *pcPombe* model (e.g. k_{cat} values, Supplementary Figure 2) and establish compartment-specific proteome constraints with pcYeast as template (Elsemman et al., 2022). We then further calibrated the *pcPombe* model with available experimental data, as explained below.

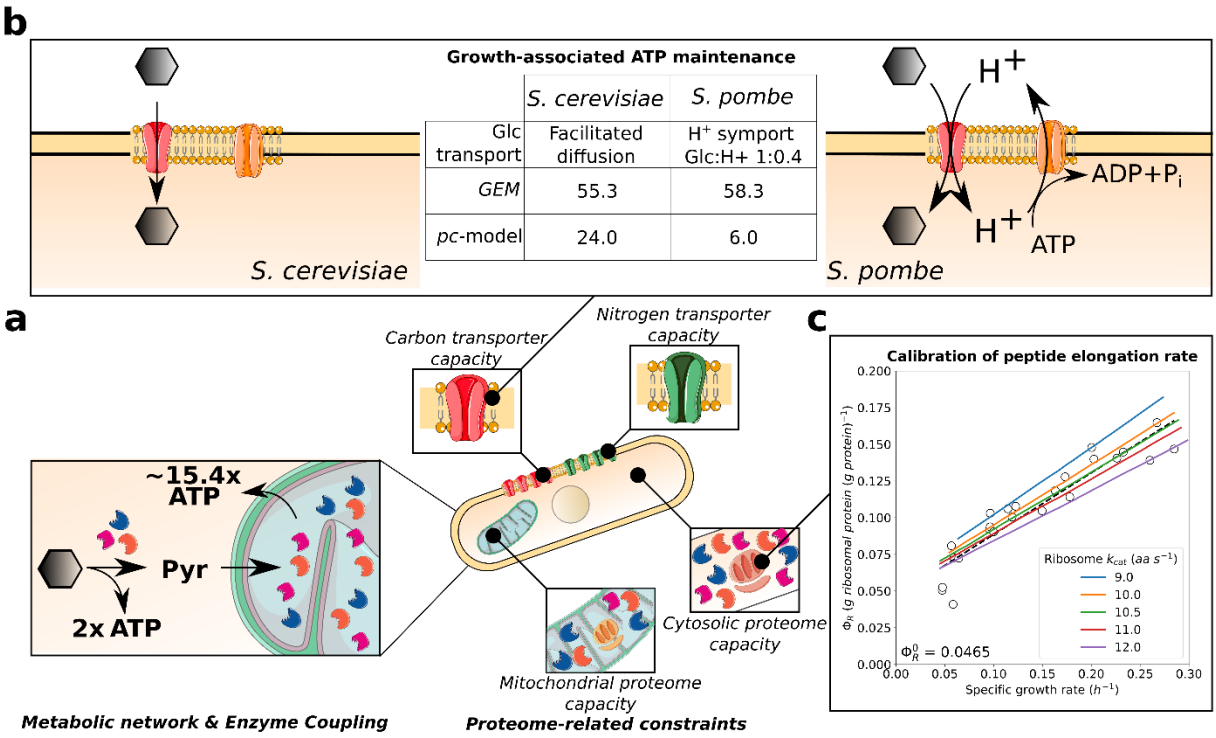

Figure 2. Calibration of the proteome-constrained model of *S. pombe*, *pcPombe*. a. The representation of different layers of the *pcPombe* model: the metabolic model (*pomGEM*) is complemented with a fine-grained description of protein turnover (reactions of protein translation, folding, degradation, and dilution by growth) and a set of compartment-specific proteome constraints (corresponding to proteome capacity of plasma membrane, mitochondria, and cytosol). **b.** Representation of the glucose transport in *S. cerevisiae* and *S. pombe*, and the estimates of ATP maintenance costs for both organisms. **c.** Calibration of the peptide elongation rate. The "inactive" fraction of ribosomes Φ_R^0 was estimated from the experimental data (black dashed line, linear fit of the experimental points), and growth on varying levels of glucose was simulated with different ribosome k_{cat} values. Abbreviations: Glc, glucose.

Calibrating ATP maintenance and protein translation costs in *pcPombe*

A substantial amount (~40% in *S. cerevisiae* (Lahtvee et al., 2017)) of ATP maintenance costs can be explained by protein turnover processes. As these processes are now modelled explicitly in the *pcPombe* model, we used the measurements of biomass yield on glucose (Figure 1c), to determine the GAM value for the *pcPombe* model (Figure 2b). We first explicitly split the ATP maintenance into two components, cytosolic and mitochondrial ATP maintenance (GAM and mitoGAM, respectively). We base this decision on the fact that mitochondria are special organelles: they have a circular genome that stores a small number of protein-coding genes, and translate them, using a distinct mitochondrial pool of ribosomes. In the model, the exact number of mitochondria per cell is not specified, therefore a practical way to express the maintenance costs is mmol ATP per gram of mitochondrial protein.

Although protein turnover cost is a major determinant of GAM, other processes, which are often not explicitly modelled, can significantly influence this value. For example, in *S. cerevisiae*, glucose enters the cell via facilitated diffusion, while di- or oligosaccharides (maltose, maltotriose, raffinose, etc.) are imported into the cell through sugar:H^+ symport, leading to additional energetic costs of using these sugars for growth (Weusthuis et al., 1993). However, in *S. pombe*, glucose transporters are also sugar:H^+ symporters, with a stoichiometry of 1:0.4 for glucose and protons, respectively (Hofer and Nassar, 1987). The actual energetic costs here come from the fact that the protons, imported with the sugar, have to be pumped out of the cell by the plasma membrane H^+-ATPases to maintain the proton balance in the cell. If this energetic cost of glucose transport is not accounted for, the growth rate will be significantly overestimated, especially during respiratory growth when the mitochondrion is used, and this is a consequence of two factors. First, by neglecting consumption of ATP by the H^+-ATPase, more ATP will be available for growth; in the model, correctly predicting the growth yield will then require a much higher GAM value. Second, increased cytosolic proton availability in the model will drive increased mitochondrial ATP synthase activity, leading to a higher ATP yield, and hence a higher estimated GAM value. We therefore added an additional constraint to the *pcPombe* model that couples glucose import to H^+-export through plasma membrane H^+-ATPases (see discussion of this modelling step in Supplementary Notes 1.4), thereby preventing incorrect use of these protons. With this additional constraint, we then estimated the ATP maintenance value.

While the GAM values for the metabolic models of *S. cerevisiae* and *S. pombe* were very similar, modification of the glucose transport mechanism resulted in a significant difference in the GAM values of the respective proteome-constrained models. In the end, we determined values of $6\ mmol\ gDW^{-1}$ and $6\ mmol\ (g\ mitochondrial\ protein)^{-1}$ for GAM and mitoGAM, respectively (Figure 2b). The estimated GAM value for *pcPombe* is thus considerably smaller than the one for *pcYeast* ($24\ mmol\ gDW^{-1}$) once the additional energetic costs of glucose transport is accounted for, (Figure 2b). For mitoGAM, the same value ($6\ mmol\ (g\ mitochondrial\ protein)^{-1}$) was used in both *pcYeast* and *pcPombe*.

Next we assessed the peptide elongation rate of the cytosolic ribosomes and the fraction of proteome, occupied by "inactive" ribosomes $\Phi_{R,0}$ (following (Metzl-Raz et al., 2017)), other key parameters, as shown for the *pcYeast* model (Elsemman et al., 2022) (Figure 2c). We used quantitative proteomics data from turbidostat experiments in EMM2 media (2% glucose), supplemented with different single nitrogen sources (Kleijn et al., 2022). First, we computed the fraction of "inactive" ribosomes $\Phi_{R,0} \approx 0.05\ g\ (g\ protein)^{-1}$ from the linear regression of the experimental data points (Figure 2c, black dashed line). Notably, the fraction of the "inactive" ribosomes is around 40% lower in *S. pombe* than in *S. cerevisiae* ($\Phi_{R,0} \approx 0.08$) (Metzl-Raz et al., 2017). Following that, we estimated the peptide elongation rate in *S. pombe*, a parameter never reported in the literature (to the best of our knowledge). We thus ran a set of model simulations, where we varied the peptide elongation rate $k_{cat,ribo}$ around the initial value of $k_{cat,ribo} = 10.5\ aa\ s^{-1}$ from *S. cerevisiae* (Metzl-Raz et al., 2017) (Figure 2c). We concluded that the

value of $10.5\ aa\ s^{-1}$ showed the best agreement with the experimental data. This suggests that although *S. cerevisiae* and *S. pombe* diverted in their evolutionary tracks relatively long time ago, their ribosomes seem to have remained highly functionally conserved.

Identifying growth-limiting proteome constraints in glucose-limited chemostats

The key feature of the *pcPombe* model is the ability to predict multiple facets of microbial physiology: flux distributions, proteome composition, and, most importantly, compartment-specific proteome constraints that actively limit the maximal growth rate. Therefore, as a use case example, we used the *pcPombe* model to identify the active constraints that drive the physiology of *S. pombe* growing in glucose-limited chemostats at increasing dilution rate (Figure 3).

We mimicked different extracellular glucose concentrations in the model by varying the saturation factor of the glucose transporters (Supplementary Notes) and used binary search (Elsemman et al., 2022) to find the maximal specific growth rate and corresponding flux distribution for every value of the saturation factor (Figure 3a). The predicted fluxes, based on external metabolites, were also used to compute the physiological parameters (yield on glucose and the respiratory quotient) of cell cultures (Figure 3b, 3c).

Based on the active compartment-specific proteome constraints (Figure 3d), we partition the simulation (along the predicted specific growth rate) into three parts (shading in all the panels of Figure 3): first, at very slow growth, the only active (i.e. the constraint expression equals 1 in Figure 3d) proteome constraint is carbon uptake (carbon transporter capacity). Carbon transporter capacity remains the only active proteome constraint before the onset of ethanol formation (critical growth rate $\mu_{crit} = 0.16\ h^{-1}$), when a second active proteome constraint is encountered, the mitochondrial proteome capacity (see below).

As growth rate continues to increase, the active constraints change (blue shaded region in Figure 3), and so does the predicted metabolic behavior. At very fast growth rates, instead of mitochondrial proteome capacity, the unspecified protein (UP) fraction (a proxy for the cytosolic proteome capacity), starts to limit growth (UP mass fraction in the proteome reaches the minimal value we estimated on the basis of proteomics data (Kleijn et al., 2022)). As a result, any increase in growth has to be accompanied by trading in mitochondrial proteins for cytosolic ones (Figure 3d, panel "Mito. capacity"). Both the minimal UP fraction and the maximal mitochondrial proteome capacity (Supplementary Notes) are estimated parameters, due to lack of supporting experimental data. We, however, believe that the sequence of active proteome constraints (thus also the fitted parameter values) is supported by literature data, coming from both *S. cerevisiae* and *S. pombe*.

First, we addressed the mitochondrial capacity being the constraint behind the onset of ethanol formation. We tested our claims by increasing the minimal UP fraction to the level that sets the maximal growth rate to $\mu^*_{max} = 0.16\ h^{-1}$ $(= \mu_{crit})$ when the glucose transporters are fully saturated and mitochondrial capacity constraint was relaxed. The flux predictions we acquired were considerably different from the experimental data and therefore we discarded such scenario. Next, we considered the active constraint (UP minimum) for growth in in glucose excess. Malina and colleagues (Malina et al., 2021) determined that both *S. cerevisiae* and *S. pombe* allocate a very similar fraction (and in both cases small, <5%) of the proteome to TCA cycle and oxidative phosphorylation proteins. This suggests that the same constraints limit growth in glucose excess, and we have previously shown that this constraint is the cytosolic proteome capacity (Elsemman et al., 2022). Therefore, the active constraints at slower growth (onset of ethanol formation) must be of a different nature, and knowledge of *S. cerevisiae* again pointed to mitochondrial proteome capacity as the constraint limiting growth at that phase. Our speculation resulted in a good flux prediction, thus we argue that it is *the* active constraint under this growth regime.

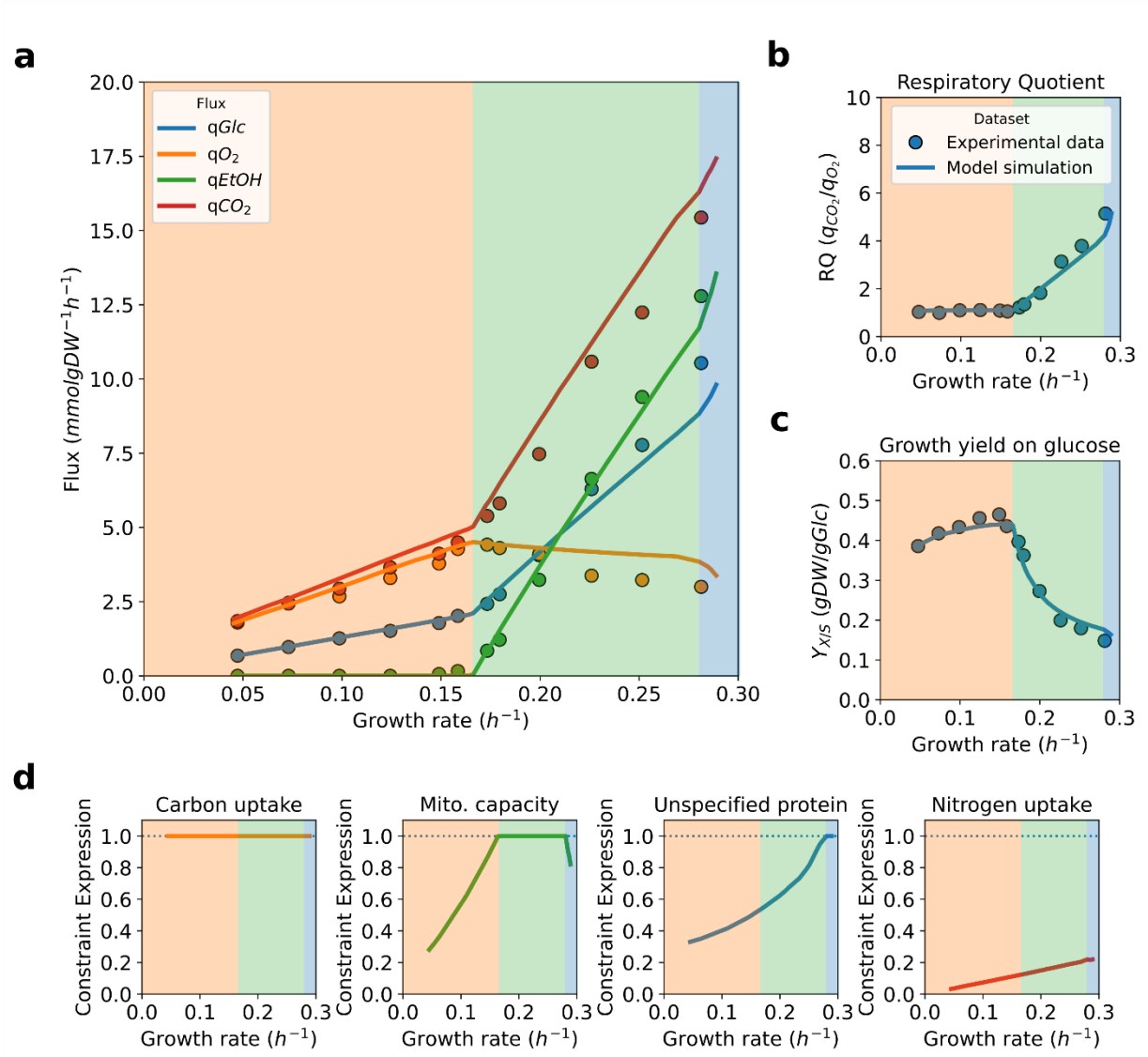

Figure 3. Fluxes, physiological parameters and active proteome constraints in glucose-limited growth of *S. pombe*. a. Main predicted fluxes from glucose-limited chemostats. **b-c.** Physiological parameters of the growth in glucose-limited chemostats: **b.** Respiratory quotient, the ratio between the specific fluxes of carbon dioxide and oxygen; **c.** Growth yield on glucose, the ratio between growth rate and glucose uptake. Experimental data (points) in panels **a-c** from (de Jong-Gubbels et al., 1996). **d.** Active proteome constraints, predicted by the *pcPombe* model. Shading of different growth regimes in panels **a-d** corresponds to active proteome constraints, plotted in panel **d**.

When the predicted growth rate approaches the maximal predicted growth rate, growth is no longer limited by carbon transporter capacity, and thus, only one constraint (minimal UP mass fraction) remains active. In this state, excretion of additional overflow products (e.g. pyruvate) is predicted, consistent with the behavior of *S. cerevisiae* at glucose excess conditions. It should be noted that the *predicted* maximal growth rate in the minimal EMM2 medium ($\mu_{max} = 0.29\ h^{-1}$) is dependent on the minimal UP fraction in the proteome, a parameter we fit. However, we argue that our estimate is reasonable, since *pcPombe*

correctly predicts the maximal growth rate on the rich YES medium with the same parameter values ($\mu_{max} = 0.34\ h^{-1}$) (Durão et al., 2021). To summarize, here we used the *pcPombe* model together with the existing knowledge on *S. cerevisiae* to verify the identity of proteome constraints, which actively limit growth in a condition-dependent manner.

Maximal growth rate of *S. pombe* is defined by limited proteome access

We observed that the maximal experimentally determined growth rate of *S. pombe* in a minimal medium ($\mu_{max} = 0.30\ h^{-1}$) is substantially lower than the maximal growth rate of *S. cerevisiae* CEN.PK strain (Verduyn medium (Verduyn et al., 1992) with glucose as carbon source, $\mu_{max} = 0.40\ h^{-1}$ (Elsemman et al., 2022)). We speculate that the lower maximal growth rate is an outcome of lower protein density in *S. pombe* biomass, and *S. cerevisiae* has a "higher budget" to accommodate proteins, needed for faster growth. *S. pombe* exhibits a constant protein density of 0.43 $g\ (gDW)^{-1}$ (de Jong-Gubbels et al., 1996), while in *S. cerevisiae*, the respective value is growth rate-dependent and is reported to be 0.505 $g\ (gDW)^{-1}$ at $\mu = 0.375\ h^{-1}$ (Canelas et al., 2011). Although different in absolute amounts, similar proteome partitioning at the maximal growth rate suggests that the maximal growth is limited by similar constraints.

The design of the *pc*-models allows for the inspection of proteome allocation in a fine-grained manner: for every enzyme that supports growth by a catalysing a metabolic flux, a corresponding *minimal* protein demand can be computed for the (hypothetical) case that all proteins work at their maximal rate: $v = [e_i] \times k_{cat,i}$. At slow growth, with low metabolic fluxes, the minimal protein demand will be low. Typically, under these conditions cells express metabolic proteins at higher levels compared to the minimal predicted protein demand (Elsemman et al., 2022; O'Brien et al., 2016). Yet, the difference decreases with increasing growth rate for *S. cerevisiae* (Elsemman et al., 2022), with a major exception of ribosomal proteins (because ribosomal parameters are fitted explicitly, Figure 2c). To illustrate the predicted proteome partitioning, we looked into the predictions of *pcPombe* at the maximal predicted growth rate, and compared the minimal predicted protein demand with experimental data (Malina et al., 2021) (Figure 4).

We used a manually-curated proteome annotation set (Supplementary Table 3) to map proteins to different functional groups or pathways. To avoid comparing >30 pathways with small proteome fractions, we grouped pathways into a handful of coarse-grained clusters (Figure 4), with an exception of glycolysis, which as directly compared as a single pathway instead of being lumped with the rest of the catabolic (pentose phosphate pathway, TCA cycle, and oxidative phosphorylation) proteins. For additional insights, we also considered the proteome composition of *S. cerevisiae* and compare this to that of *S. pombe*. For both model predicted and experimentally determined proteome fractions, most of these coarse-grained clusters occupy comparable sized proteome fractions in both organisms. Also the deviations between predicted minimal protein demand and experimental protein fraction have similar patterns in both organisms. When looking at predictions a significant deviation from experimental data is seen in the proteome fraction involved in the metabolism of carbohydrates. The experimentally determined fraction of glycolytic enzymes is 2-fold higher than the predicted minimal demand.

This result is not completely surprising, since we observed a similar result (ca. 2-fold) in previously published proteome data of *S. cerevisiae* cultures at the maximal growth rate in minimal medium (batch cultures with excess glucose) (Elsemman et al., 2022). It appears therefore that both these yeasts have an overcapacity of glycolytic enzymes that is not needed to support the maximal growth rate; why this is the case, is currently not understood. Overall, we observed that the proteome partitioning at maximal growth is similar between *S. pombe* and *S. cerevisiae*. This supports the inference that the maximal growth under

nutrient excess is limited by a similar constraint in both organisms. Following the predictions of proteome-constrained models, we suggest that this constraint is total proteome capacity.

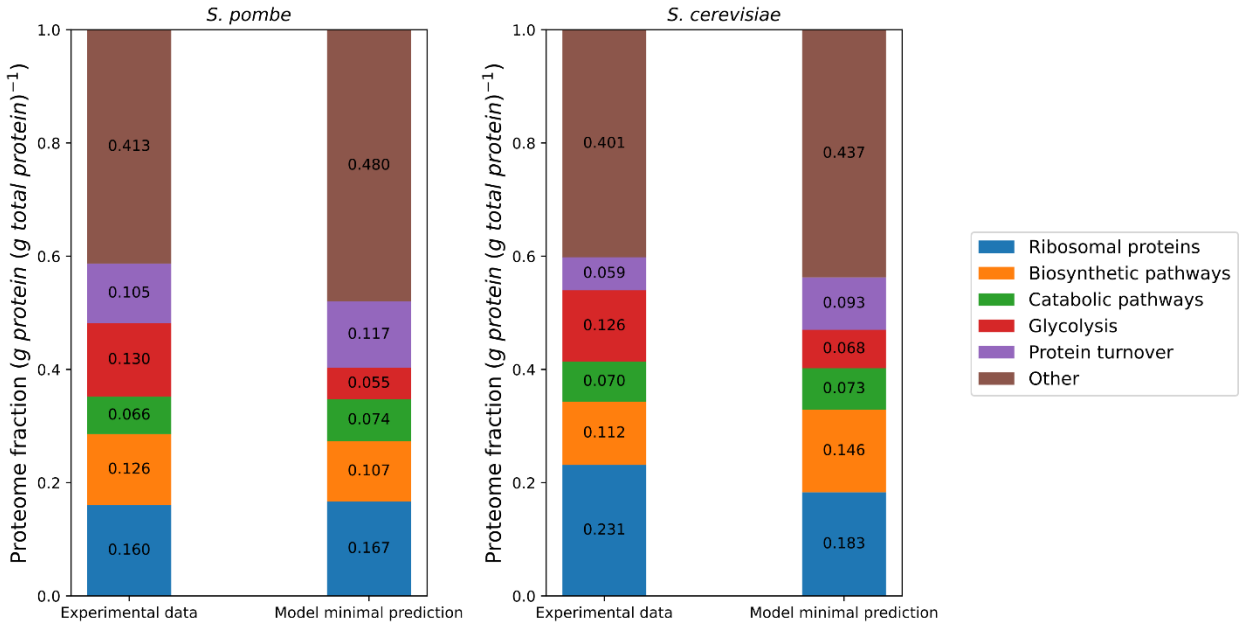

Figure 4. Proteome composition of *S. pombe* and *S. cerevisiae* at maximal growth rate. Experimentally measured proteome composition (left bars) and predicted minimal protein level (right bars) represented as proteome mass fractions, in $g\ (g\ protein)^{-1}$. Experimental data for both *S. pombe* and *S. cerevisiae* were taken from (Malina et al., 2021), and model predictions for *S. cerevisiae* taken from (Elsemman et al., 2022). Experimentally determined proteome composition in the Figure corresponds to the average of measurements reported in (Malina et al., 2021).

Discussion

In this study, we used metabolic modelling and data from the well-studied budding yeast, *S. cerevisiae,* to gain insights into the metabolism and physiology of the distantly related fission yeast, *S. pombe*. As a result, we presented a computational toolbox to investigate fission yeast metabolism at genome scale. Two types of models, in our view, are required to cover this need: a genome-scale metabolic model (metabolic potential) and a proteome-constrained (pc-) model (resource allocation).

Here we first developed a manually-curated and calibrated GEM, *pomGEM*, based on a metabolic model of budding yeast *S. cerevisiae* (Lu et al., 2019) (Figure 1). As an outcome of the model calibration, in this manuscript we provide for the first time a comprehensive and data-supported estimate of growth-associated maintenance (GAM) costs of *S. pombe* (Figure 1c). An earlier proposed GAM value of $17.37\ mmol\ gDW^{-1}$ (Sohn et al., 2012) corresponds to an unrealistically high yield of biomass on glucose in aerobic settings, while our proposed value ($58.3\ mmol\ gDW^{-1}$) corresponds well with existing experimental data. Moreover, the GAM value we estimated is very close to that reported for *S. cerevisiae* ($55.3\ mmol\ gDW^{-1}$) (Famili et al., 2003), further supporting our estimate over previous estimates (Sohn et al., 2012).

We benchmarked the *pomGEM* model by first predicting growth on single carbon sources (with only one false-negative, Figure 1d), lethal single-gene KOs (Figure 1e), and single-reaction KOs (Supplementary

Table 3). For the latter, the fraction of true predictions was approximately 74%, a good improvement on the previously reported model (61.2%) (Sohn et al., 2012). However, in the same study, the authors of the *SpoMBEL1693* model reported an increase in the true prediction rate up to 82.7%, after significant manual curation. Here, the authors "reconciled" the false predictions which arise from, e.g. duplicate reactions present in other compartments, or dead-end pathways to achieve the higher true prediction rate. However, such *ad hoc* approach requires supporting experimental data to resolve every false prediction reliably. Nonetheless, following the evolution of true prediction rates of the *S. cerevisiae* models – in terms of genes – (90.3% in Yeast8 vs 83.6% in Yeast4 (Dobson et al., 2010)), or the latest GEM of *E. coli* (>90%, (Monk et al., 2017), it is anticipated that with more experimental data, future iterations of *pomGEM* will similarly lead to further improvements in the true prediction rate.

Then, on the basis of *pomGEM,* and with *pcYeast* as template (Elsemman et al., 2022), we reconstructed (Figure 2a) and calibrated (Figure 2b, 2c) a proteome-constrained metabolic model of *S. pombe*, *pcPombe*. We first identified a major ATP maintenance component: plasma membrane H^+-ATPase activity, required to export protons that are imported through glucose:H^+ symport (Figure 2b). We also estimated the peptide elongation rate of cytosolic ribosomes, and found this to be similar to the rate reported for *S. cerevisiae* (Figure 2c).

We used the *pcPombe* model to simulate the physiology of *S. pombe* in glucose-limited chemostats at different dilution rates (Figure 3) and identified proteome constraints that actively limit growth. Despite a large evolutionary distance, constraints similar to those recently described for *S. cerevisiae* (Elsemman et al., 2022) were shown to dictate growth behaviours, with a mitochondrial proteome capacity limitation ultimately driving a switch from respiration to fermentation. Finally, we looked at the predicted minimal proteome demand at the maximal growth rate of *S. pombe* in minimal medium, and compared it to experimental measurements (Figure 4). For many coarse-grained proteome clusters, minimal predicted demands were comparable, and the prediction outcome was similar to that of *S. cerevisiae* at maximal growth rate in minimal medium. Such agreement suggests that the growth in nutrient excess is limited by similar constraints in both organisms, in this case, total proteome capacity constraint. A notable exception in predicted minimal demand vs. experimental data was seen for glycolysis, where an experimentally determined proteome fraction was 2--fold higher than the minimal predicted demand. This result suggests a large over-capacity of glycolytic enzymes, also found for *S. cerevisiae* (Elsemman et al., 2022). However, the reason for this over-capacity remains to be resolved.

Quantitative differences in proteome composition, especially at individual protein level, between the model and experimental measurements (likewise large or small), can be influenced by several factors. First, we consider the minimal protein demand in the model. This assumption ignores any preparatory protein expression, and the predicted protein abundance is highly dependent on the k_{cat} values. The effects of other kinetic factors are also not accounted for, e.g. suboptimal saturation of enzymes and feedback effects (positive and negative alike) in the biochemical pathways. Therefore, protein "underutilization" (or "reserve capacity") is a frequently-observed prediction of resource allocation models (Elsemman et al., 2022; O'Brien et al., 2016). Second, GEMs consider only proteins with direct metabolic function (plus those directly related to protein turnover, in the *pcPombe* model). Thus, some proteins will be unaccounted for when mapping them to annotated pathways. Improved GPR annotations in future version(s) of *pomGEM* would reduce such "lost" mappings.

Throughout the manuscript, we considered very few applications of the computational toolbox, and only a handful of data sources. This is because the predictive power of current *pomGEM* and *pcPombe* models is severely hampered by a lack of consistent, high-quality experimental datasets in order to calibrate and validate the models. The hope is that our current effort to provide a computational tool to study *S.*

pombe's metabolism will stimulate an iterative cycle of hypothesis generation, experimental testing and model refinement. For *S. cerevisiae*, its genome-scale model is already in its 8th iteration, with efforts beginning almost two decades ago (Famili et al., 2003). Throughout the years, essential modelling parameters, such as the GAM value (Famili et al., 2003), growth rate-dependent biomass composition (Canelas et al., 2011), ribosome peptide elongation rate (Metzl-Raz et al., 2017), and a large panel of kinetic parameters (used in e.g. (Lu et al., 2019; Nilsson and Nielsen, 2016)), were determined. Thus, by aggregating a vast amount of existing literature data, and acquiring new experimental datasets (physiological data and proteomics), a proteome-constrained model of *S. cerevisiae* (*pcYeast*) was created and could be successfully tested in a number of scenarios ((Elsemman et al., 2022), Grigaitis et al., unpublished).

Existing experimental datasets of *S. pombe*, unfortunately, are not as comprehensive. Although many of the datasets are of high-quality, they consider only one aspect of cell growth, for instance, exometabolite fluxes (de Jong-Gubbels et al., 1996), or proteome composition (Kleijn et al., 2022). For modelling purposes, systemic experiments which cover several layers of information at once (e.g. sampling from the same cultures to quantify bulk biomass composition, exometabolite fluxes, and proteome composition), as well as testing current predictions on active proteome constraints by e.g. titrating expression of non-functional proteins targeted to specific cell compartments (e.g. cytoplasm, cell membrane etc.), as has been done for *E. coli* (Scott *et al.*, (Scott et al., 2010)), or by testing optimal protein allocation with evolution experiments (as performed in e.g. *Lactococcus lactis* (Chen et al., 2021)) will be extremely useful. Performing such experiments and subsequent model refinements will have great influence on the predictive power of the *pomGEM* and *pcPombe* models and will pave the way towards deeper understanding of metabolism and resource allocation of fission yeast *Schizosaccharomyces pombe*.

Lastly, recent studies suggested *S. pombe* could find novel applications in biotechnology, including winemaking (Benito et al., 2016) and flavour formation during food fermentations (Du et al., 2021), but also as a possible cell factory (Madhavan et al., 2021). *S. pombe*'s ability to grow in environments with low water activity, high alcohol content, very low pH and a wide range of temperatures (Loira et al., 2018) make it an attractive, and perhaps underutilized, biotechnological tool. However, identifying metabolic engineering targets and predicting outcomes is a major challenge without a robust computational framework. The two models we present here, therefore, are powerful tools that can be used to efficiently explore, *in silico*, *S. pombe's* metabolic potential, to identify metabolic engineering targets, to design and optimize medium for different applications, and to study metabolic and physiological determinants of growth behaviour under different growth conditions.

Methods

Determination of growth on different carbon sources

Schizosaccharomyces pombe strain CBS1042 (Westerdijk Fungal Biodiversity Institute, The Netherlands) was used to determine growth capacity on different individual carbon sources. Glycerol stocks were prepared from cells grown to saturation in YPD medium and stored at -80˚C. All cultures were performed at 30˚C using EMM2 (Hagan et al., 2016) as a base medium. All carbon source concentrations are expressed as carbon mol (C-mM), and were added to a final concentration of 600 C-mM (e.g. 100 mM glucose, 50 mM sucrose, 200 mM pyruvate etc.). Growth experiments were carried out using a SpectraMax Plus 384 microplate reader (Molecular Devices, Silicon Valley, California). A standardized procedure was used for revival and inoculation of cultures. Briefly, glycerol stocks were revived by 100 times diluted inoculation into EMM2 with 600 C-mM glucose. After approximately 7 hrs, overnight cultures were again diluted and inoculated into EMM2 + glucose to a final OD_{600nm} of 0.02. The next day, fresh media containing the carbon

sources to be tested (Table S1) were inoculated to a final OD_{600nm} of 0.01. After 6 hrs, cultures were again diluted (final OD_{600nm} of 0.01) using the same medium and transferred to 96-well microtitre plates. Per carbon source, 10 technical replicates were included (300 µl per well), along with 5 negative controls (growth medium with carbon source, no cells). Temperature was set to 30˚C and double orbital shaking at 600 rpm was used. OD values were recorded at 5-minute intervals at 600 nm for approximately 80 hrs.

Reconstruction of the metabolic network of *Schizosaccharomyces pombe*

The metabolic network of *S. pombe* was reconstructed with CBMPy MetaDraft (Olivier et al., 2020), using the reference proteome sequence from PomBase (Lock et al., 2019) and Yeast8.3.3 (Lu et al., 2019) as the template model. Model simulations, as well as manual refinement and gap-filling were performed in CBMPy 0.8.2 (Olivier et al., 2021) under Python 3.9 environment with IBM ILOG CPLEX 20.10 as the linear program (LP) solver.

Mapping essential reactions to gene lethality

Essential reactions in the model were determined by computing the predicted growth rate with a single reaction being blocked (lower and upper flux bounds set to 0.0) for all reactions in the model. If blocked flux through a reaction resulted in a predicted growth rate 90% or lower of the maximal (wild-type) growth rate, we considered such reaction essential; otherwise, the mutant is considered viable. Only reactions with existing gene-protein-reaction (GPR) associations were considered and compared with experimental data. For GPRs containing an "OR" clause, the experimentally determined essentiality has to match for all listed genes (or combinations of) to be assigned either "viable" or "essential". For GPRs containing an "AND" clause, reaction is assigned "essential" if at least one of the genes is experimentally determined to be essential; "viable" is assigned the same way as for "OR" clauses. Conflicting results or missing essentiality experiments were labelled "ambiguous" and not considered further.

Reconstruction and simulations of the proteome-constrained model

The detailed description of reconstruction of the proteome-constrained model of *S. pombe* is provided in the Supplementary Notes. We used the reference proteome of *S. pombe* from UniProt (The UniProt Consortium et al., 2021). Proteomes and kinetic data (enzyme turnover values) were collected from the BRENDA database (Chang et al., 2021). 5'-UTR sequences and proteome annotations (composition of macromolecular complexes, Gene Ontology terms etc.) were collected from PomBase (Lock et al., 2019). The *pcPombe* model was simulated using CBMPy 0.8.2 (Olivier et al., 2021) under Python 3.9 environment with IBM ILOG CPLEX 20.10 and SoPlex 4.0 (Gleixner et al., 2018) as the low- and high-precision LP solver, respectively.

Acknowledgements

We thank Istvan T. Kleijn (Imperial College London, the United Kingdom) for sharing unpublished transcriptomics and proteomics data and discussions, Brett G. Olivier for his help on the modelling software, and Julius Battjes for discussions. PG acknowledges support by Marie Skłodowska-Curie Actions ITN "SynCrop" (grant agreement No 764591). EvPK and BT acknowledge funding from the Netherlands Organisation for Scientific Research (grant No ALWTF.2015.4). We thank SURFsara for the HPC resources through access to the Lisa Compute Cluster.

Data and Code Availability

Experimental data on growth of *S. pombe* on different carbon sources is provided in Supplementary Table 1. The *pomGEM* model, *pcPombe* model, and the materials to generate *pcPombe* model, together with information, required to generate the figures of this manuscript, are available on Zenodo [10.5281/zenodo.6513463].

Author Contributions

Conceptualization, funding acquisition and supervision: BT, JHvH; experimental data collection and analysis: PG, MI, GX, JHvH; computational modeling: PG, DG, EvPK; formal analysis and software: PG, DG, EvPK, SMF, JHvH; writing – original draft: PG; writing – editing: PG, EvPK, BT, JHvH. All authors have read and approved the manuscript.

Competing Interests Statement

The project is partly organised by and executed under the auspices of TiFN, a public – private partnership on precompetitive research in food and nutrition. Among other sources declared, funding for this research (to EvPK and BT) was obtained from Friesland Campina, CSK Food Enrichment and the Netherlands Organisation for Scientific Research. The authors have declared that no competing interests exist in the writing of this publication.

References

Benito, Á., Jeffares, D., Palomero, F., Calderón, F., Bai, F.-Y., Bähler, J., Benito, S., 2016. Selected Schizosaccharomyces pombe Strains Have Characteristics That Are Beneficial for Winemaking. PLOS ONE 11, e0151102. https://doi.org/10.1371/journal.pone.0151102

Beste, D.J., Hooper, T., Stewart, G., Bonde, B., Avignone-Rossa, C., Bushell, M.E., Wheeler, P., Klamt, S., Kierzek, A.M., McFadden, J., 2007. GSMN-TB: a web-based genome-scale network model of Mycobacterium tuberculosis metabolism. Genome Biol. 8, R89. https://doi.org/10.1186/gb-2007-8-5-r89

Branco dos Santos, F., Olivier, B.G., Boele, J., Smessaert, V., De Rop, P., Krumpochova, P., Klau, G.W., Giera, M., Dehottay, P., Teusink, B., Goffin, P., 2017. Probing the Genome-Scale Metabolic Landscape of Bordetella pertussis, the Causative Agent of Whooping Cough. Appl. Environ. Microbiol. 83. https://doi.org/10.1128/AEM.01528-17

Canelas, A.B., Ras, C., ten Pierick, A., van Gulik, W.M., Heijnen, J.J., 2011. An in vivo data-driven framework for classification and quantification of enzyme kinetics and determination of apparent thermodynamic data. Metab. Eng. 13, 294–306. https://doi.org/10.1016/j.ymben.2011.02.005

Chang, A., Jeske, L., Ulbrich, S., Hofmann, J., Koblitz, J., Schomburg, I., Neumann-Schaal, M., Jahn, D., Schomburg, D., 2021. BRENDA, the ELIXIR core data resource in 2021: new developments and updates. Nucleic Acids Res. 49, D498–D508. https://doi.org/10.1093/nar/gkaa1025

Chen, Y., Nielsen, J., 2019. Energy metabolism controls phenotypes by protein efficiency and allocation. Proc. Natl. Acad. Sci. 116, 17592–17597. https://doi.org/10.1073/pnas.1906569116

Chen, Y., Pelt-KleinJan, E., Olst, B., Douwenga, S., Boeren, S., Bachmann, H., Molenaar, D., Nielsen, J., Teusink, B., 2021. Proteome constraints reveal targets for improving microbial fitness in nutrient-rich environments. Mol. Syst. Biol. 17. https://doi.org/10.15252/msb.202010093

Choi, G.-W., Um, H.-J., Kim, M., Kim, Y., Kang, H.-W., Chung, B.-W., Kim, Y.-H., 2010. Isolation and characterization of ethanol-producing Schizosaccharomyces pombe CHFY0201. J. Microbiol. Biotechnol. 20, 828–834.

De Becker, K., Totis, N., Bernaerts, K., Waldherr, S., 2022. Using resource constraints derived from genomic and proteomic data in metabolic network models. Curr. Opin. Syst. Biol. 29, 100400. https://doi.org/10.1016/j.coisb.2021.100400

de Groot, D.H., Lischke, J., Muolo, R., Planqué, R., Bruggeman, F.J., Teusink, B., 2020. The common message of constraint-based optimization approaches: overflow metabolism is caused by two growth-limiting constraints. Cell. Mol. Life Sci. 77, 441–453. https://doi.org/10.1007/s00018-019-03380-2

de Jong-Gubbels, P., van Dijken, J.P., Pronk, J.T., 1996. Metabolic fluxes in chernostat cultures of Schizosaccharomyces pombe grown on mixtures of glucose and ethanol. Microbiology 142, 1399–1407. https://doi.org/10.1099/13500872-142-6-1399

de Queiroz, J.H., Uribelarrea, J.-L., Pareilleux, A., 1993. Estimation of the energetic biomass yield and efficiency of oxidative phosphorylation in cell-recycle cultures of Schizosaccharomyces pombe. Appl. Microbiol. Biotechnol. 39, 609–614. https://doi.org/10.1007/BF00205061

Dobson, P.D., Smallbone, K., Jameson, D., Simeonidis, E., Lanthaler, K., Pir, P., Lu, C., Swainston, N., Dunn, W.B., Fisher, P., Hull, D., Brown, M., Oshota, O., Stanford, N.J., Kell, D.B., King, R.D., Oliver, S.G., Stevens, R.D., Mendes, P., 2010. Further developments towards a genome-scale metabolic model of yeast. BMC Syst. Biol. 4, 145. https://doi.org/10.1186/1752-0509-4-145

Du, H., Song, Z., Zhang, M., Nie, Y., Xu, Y., 2021. The deletion of Schizosaccharomyces pombe decreased the production of flavor-related metabolites during traditional Baijiu fermentation. Food Res. Int. 140, 109872. https://doi.org/10.1016/j.foodres.2020.109872

503 Dukovski, I., Bajić, D., Chacón, J.M., Quintin, M., Vila, J.C.C., Sulheim, S., Pacheco, A.R., Bernstein, D.B.,
504 Riehl, W.J., Korolev, K.S., Sanchez, A., Harcombe, W.R., Segrè, D., 2021. A metabolic modeling
505 platform for the computation of microbial ecosystems in time and space (COMETS). Nat. Protoc.
506 16, 5030–5082. https://doi.org/10.1038/s41596-021-00593-3
507 Durão, P., Amicone, M., Perfeito, L., Gordo, I., 2021. Competition dynamics in long-term propagations of
508 *Schizosaccharomyces pombe* strain communities. Ecol. Evol. 11, 15085–15097.
509 https://doi.org/10.1002/ece3.8191
510 Elsemman, I.E., Rodriguez Prado, A., Grigaitis, P., Garcia Albornoz, M., Harman, V., Holman, S.W., van
511 Heerden, J., Bruggeman, F.J., Bisschops, M.M.M., Sonnenschein, N., Hubbard, S., Beynon, R.,
512 Daran-Lapujade, P., Nielsen, J., Teusink, B., 2022. Whole-cell modeling in yeast predicts
513 compartment-specific proteome constraints that drive metabolic strategies. Nat. Commun. 13,
514 801. https://doi.org/10.1038/s41467-022-28467-6
515 Famili, I., Forster, J., Nielsen, J., Palsson, B.O., 2003. Saccharomyces cerevisiae phenotypes can be
516 predicted by using constraint-based analysis of a genome-scale reconstructed metabolic
517 network. Proc. Natl. Acad. Sci. 100, 13134–13139. https://doi.org/10.1073/pnas.2235812100
518 Fang, X., Lloyd, C.J., Palsson, B.O., 2020. Reconstructing organisms in silico: genome-scale models and
519 their emerging applications. Nat. Rev. Microbiol. 18, 731–743. https://doi.org/10.1038/s41579-
520 020-00440-4
521 Forsburg, S.L., Nurse, P., 1991. Cell Cycle Regulation in the Yeasts *Saccharomyces cerevisiae* and
522 *Schizosaccharomyces pombe*. Annu. Rev. Cell Biol. 7, 227–256.
523 https://doi.org/10.1146/annurev.cb.07.110191.001303
524 Gleixner, A., Bastubbe, M., Eifler, L., Gally, T., Gamrath, G., Gottwald, R.L., Hendel, G., Hojny, C., Koch, T.,
525 Lübbecke, M., Maher, S.J., Miltenberger, M., Müller, B., Pfetsch, M., Puchert, C., Rehfeldt, D.,
526 Schlösser, F., Schubert, C., Serrano, F., Shinano, Y., Viernickel, J.M., Walter, M., Wegscheider, F.,
527 Witt, J.T., Witzig, J., 2018. The SCIP Optimization Suite 6.0 (No. 18–26). ZIB, Takustr. 7, 14195
528 Berlin.
529 Hagan, I.M., Grallert, A., Simanis, V., 2016. Synchronizing Progression of *Schizosaccharomyces pombe*
530 Cells from G $_2$ through Repeated Rounds of Mitosis and S Phase with *cdc25-22* Arrest Release.
531 Cold Spring Harb. Protoc. 2016, pdb.prot091264. https://doi.org/10.1101/pdb.prot091264
532 Hofer, M., Nassar, F.R., 1987. Aerobic and Anaerobic Uptake of Sugars in Schizosaccharomyces pombe.
533 Microbiology 133, 2163–2172. https://doi.org/10.1099/00221287-133-8-2163
534 Hoffman, C.S., Wood, V., Fantes, P.A., 2015. An Ancient Yeast for Young Geneticists: A Primer on the
535 *Schizosaccharomyces pombe* Model System. Genetics 201, 403–423.
536 https://doi.org/10.1534/genetics.115.181503
537 Kim, D.-U., Hayles, J., Kim, D., Wood, V., Park, H.-O., Won, M., Yoo, H.-S., Duhig, T., Nam, M., Palmer, G.,
538 Han, S., Jeffery, L., Baek, S.-T., Lee, H., Shim, Y.S., Lee, M., Kim, L., Heo, K.-S., Noh, E.J., Lee, A.-R.,
539 Jang, Y.-J., Chung, K.-S., Choi, S.-J., Park, J.-Y., Park, Y., Kim, H.M., Park, S.-K., Park, H.-J., Kang, E.-
540 J., Kim, H.B., Kang, H.-S., Park, H.-M., Kim, K., Song, K., Song, K.B., Nurse, P., Hoe, K.-L., 2010.
541 Analysis of a genome-wide set of gene deletions in the fission yeast Schizosaccharomyces
542 pombe. Nat. Biotechnol. 28, 617–623. https://doi.org/10.1038/nbt.1628
543 Kim, H.U., Kim, S.Y., Jeong, H., Kim, T.Y., Kim, J.J., Choy, H.E., Yi, K.Y., Rhee, J.H., Lee, S.Y., 2011.
544 Integrative genome-scale metabolic analysis of *Vibrio vulnificus* for drug targeting and discovery.
545 Mol. Syst. Biol. 7, 460. https://doi.org/10.1038/msb.2010.115
546 Kleijn, I.T., Martínez-Segura, A., Bertaux, F., Saint, M., Kramer, H., Shahrezaei, V., Marguerat, S., 2022.
547 Growth-rate-dependent and nutrient-specific gene expression resource allocation in fission
548 yeast. Life Sci. Alliance 5, e202101223. https://doi.org/10.26508/lsa.202101223

549 Klein, T., Heinzle, E., Schneider, K., 2013. Metabolic fluxes in Schizosaccharomyces pombe grown on
550 glucose and mixtures of glycerol and acetate. Appl. Microbiol. Biotechnol. 97, 5013–5026.
551 https://doi.org/10.1007/s00253-013-4718-z
552 Lahtvee, P.-J., Sánchez, B.J., Smialowska, A., Kasvandik, S., Elsemman, I.E., Gatto, F., Nielsen, J., 2017.
553 Absolute Quantification of Protein and mRNA Abundances Demonstrate Variability in Gene-
554 Specific Translation Efficiency in Yeast. Cell Syst. 4, 495-504.e5.
555 https://doi.org/10.1016/j.cels.2017.03.003
556 Lock, A., Rutherford, K., Harris, M.A., Hayles, J., Oliver, S.G., Bähler, J., Wood, V., 2019. PomBase 2018:
557 user-driven reimplementation of the fission yeast database provides rapid and intuitive access
558 to diverse, interconnected information. Nucleic Acids Res. 47, D821–D827.
559 https://doi.org/10.1093/nar/gky961
560 Loira, I., Morata, A., Palomero, F., González, C., Suárez-Lepe, J., 2018. Schizosaccharomyces pombe: A
561 Promising Biotechnology for Modulating Wine Composition. Fermentation 4, 70.
562 https://doi.org/10.3390/fermentation4030070
563 Lu, H., Li, F., Sánchez, B.J., Zhu, Z., Li, G., Domenzain, I., Marcišauskas, S., Anton, P.M., Lappa, D., Lieven,
564 C., Beber, M.E., Sonnenschein, N., Kerkhoven, E.J., Nielsen, J., 2019. A consensus S. cerevisiae
565 metabolic model Yeast8 and its ecosystem for comprehensively probing cellular metabolism.
566 Nat. Commun. 10, 3586. https://doi.org/10.1038/s41467-019-11581-3
567 Lu, H., Li, F., Yuan, L., Domenzain, I., Yu, R., Wang, H., Li, G., Chen, Y., Ji, B., Kerkhoven, E.J., Nielsen, J.,
568 2021. Yeast metabolic innovations emerged via expanded metabolic network and gene positive
569 selection. Mol. Syst. Biol. 17. https://doi.org/10.15252/msb.202110427
570 Madhavan, A., Arun, K.B., Sindhu, R., Krishnamoorthy, J., Reshmy, R., Sirohi, R., Pugazhendi, A., Awasthi,
571 M.K., Szakacs, G., Binod, P., 2021. Customized yeast cell factories for biopharmaceuticals: from
572 cell engineering to process scale up. Microb. Cell Factories 20, 124.
573 https://doi.org/10.1186/s12934-021-01617-z
574 Malina, C., Yu, R., Björkeroth, J., Kerkhoven, E.J., Nielsen, J., 2021. Adaptations in metabolism and
575 protein translation give rise to the Crabtree effect in yeast. Proc. Natl. Acad. Sci. 118,
576 e2112836118. https://doi.org/10.1073/pnas.2112836118
577 McAnulty, M.J., Yen, J.Y., Freedman, B.G., Senger, R.S., 2012. Genome-scale modeling using flux ratio
578 constraints to enable metabolic engineering of clostridial metabolism in silico. BMC Syst. Biol. 6,
579 42. https://doi.org/10.1186/1752-0509-6-42
580 Metzl-Raz, E., Kafri, M., Yaakov, G., Soifer, I., Gurvich, Y., Barkai, N., 2017. Principles of cellular resource
581 allocation revealed by condition-dependent proteome profiling. eLife 6, e28034.
582 https://doi.org/10.7554/eLife.28034
583 Mishra, P., Lee, N.-R., Lakshmanan, M., Kim, M., Kim, B.-G., Lee, D.-Y., 2018. Genome-scale model-driven
584 strain design for dicarboxylic acid production in Yarrowia lipolytica. BMC Syst. Biol. 12, 12.
585 https://doi.org/10.1186/s12918-018-0542-5
586 Monk, J.M., Lloyd, C.J., Brunk, E., Mih, N., Sastry, A., King, Z., Takeuchi, R., Nomura, W., Zhang, Z., Mori,
587 H., Feist, A.M., Palsson, B.O., 2017. iML1515, a knowledgebase that computes Escherichia coli
588 traits. Nat. Biotechnol. 35, 904–908. https://doi.org/10.1038/nbt.3956
589 Nilsson, A., Nielsen, J., 2016. Metabolic Trade-offs in Yeast are Caused by F1F0-ATP synthase. Sci. Rep. 6,
590 22264. https://doi.org/10.1038/srep22264
591 O'Brien, E.J., Utrilla, J., Palsson, B.O., 2016. Quantification and Classification of E. coli Proteome
592 Utilization and Unused Protein Costs across Environments. PLOS Comput. Biol. 12, e1004998.
593 https://doi.org/10.1371/journal.pcbi.1004998
594 Olivier, B., Gottstein, W., Molenaar, D., Teusink, B., 2021. CBMPy release 0.8.2. Zenodo.
595 https://doi.org/10.5281/ZENODO.5546608

596 Olivier, B.G., Mendoza, S., Molenaar, D., Teusink, B., 2020. MetaDraft Release: 0.9.5. Zenodo.
597 https://doi.org/10.5281/ZENODO.4291058
598 Pitkänen, E., Jouhten, P., Hou, J., Syed, M.F., Blomberg, P., Kludas, J., Oja, M., Holm, L., Penttilä, M.,
599 Rousu, J., Arvas, M., 2014. Comparative Genome-Scale Reconstruction of Gapless Metabolic
600 Networks for Present and Ancestral Species. PLoS Comput. Biol. 10, e1003465.
601 https://doi.org/10.1371/journal.pcbi.1003465
602 Scott, M., Gunderson, C.W., Mateescu, E.M., Zhang, Z., Hwa, T., 2010. Interdependence of Cell Growth
603 and Gene Expression: Origins and Consequences. Science 330, 1099–1102.
604 https://doi.org/10.1126/science.1192588
605 Sohn, S.B., Kim, T.Y., Lee, J.H., Lee, S.Y., 2012. Genome-scale metabolic model of the fission yeast
606 Schizosaccharomyces pombe and the reconciliation of in silico/in vivo mutant growth. BMC Syst.
607 Biol. 6, 49. https://doi.org/10.1186/1752-0509-6-49
608 The UniProt Consortium, Bateman, A., Martin, M.-J., Orchard, S., Magrane, M., Agivetova, R., Ahmad, S.,
609 Alpi, E., Bowler-Barnett, E.H., Britto, R., Bursteinas, B., Bye-A-Jee, H., Coetzee, R., Cukura, A., Da
610 Silva, A., Denny, P., Dogan, T., Ebenezer, T., Fan, J., Castro, L.G., Garmiri, P., Georghiou, G.,
611 Gonzales, L., Hatton-Ellis, E., Hussein, A., Ignatchenko, A., Insana, G., Ishtiaq, R., Jokinen, P.,
612 Joshi, V., Jyothi, D., Lock, A., Lopez, R., Luciani, A., Luo, J., Lussi, Y., MacDougall, A., Madeira, F.,
613 Mahmoudy, M., Menchi, M., Mishra, A., Moulang, K., Nightingale, A., Oliveira, C.S., Pundir, S.,
614 Qi, G., Raj, S., Rice, D., Lopez, M.R., Saidi, R., Sampson, J., Sawford, T., Speretta, E., Turner, E.,
615 Tyagi, N., Vasudev, P., Volynkin, V., Warner, K., Watkins, X., Zaru, R., Zellner, H., Bridge, A., Poux,
616 S., Redaschi, N., Aimo, L., Argoud-Puy, G., Auchincloss, A., Axelsen, K., Bansal, P., Baratin, D.,
617 Blatter, M.-C., Bolleman, J., Boutet, E., Breuza, L., Casals-Casas, C., de Castro, E., Echioukh, K.C.,
618 Coudert, E., Cuche, B., Doche, M., Dornevil, D., Estreicher, A., Famiglietti, M.L., Feuermann, M.,
619 Gasteiger, E., Gehant, S., Gerritsen, V., Gos, A., Gruaz-Gumowski, N., Hinz, U., Hulo, C., Hyka-
620 Nouspikel, N., Jungo, F., Keller, G., Kerhornou, A., Lara, V., Le Mercier, P., Lieberherr, D.,
621 Lombardot, T., Martin, X., Masson, P., Morgat, A., Neto, T.B., Paesano, S., Pedruzzi, I., Pilbout, S.,
622 Pourcel, L., Pozzato, M., Pruess, M., Rivoire, C., Sigrist, C., Sonesson, K., Stutz, A., Sundaram, S.,
623 Tognolli, M., Verbregue, L., Wu, C.H., Arighi, C.N., Arminski, L., Chen, C., Chen, Y., Garavelli, J.S.,
624 Huang, H., Laiho, K., McGarvey, P., Natale, D.A., Ross, K., Vinayaka, C.R., Wang, Q., Wang, Y.,
625 Yeh, L.-S., Zhang, J., Ruch, P., Teodoro, D., 2021. UniProt: the universal protein knowledgebase
626 in 2021. Nucleic Acids Res. 49, D480–D489. https://doi.org/10.1093/nar/gkaa1100
627 Uribelarrea, J.L., De Queiroz, H., Goma, G., Pareilleux, A., 1993. Carbon and energy balances in cell-
628 recycle cultures ofSchizosaccharomyces pombe. Biotechnol. Bioeng. 42, 729–736.
629 https://doi.org/10.1002/bit.260420608
630 Uribelarrea, J.-L., De Queiroz, J.H., Pareilleux, A., 1997. Growth ofschizosaccharomyces pombe on
631 glucose-malte mixtures in continuous cell-recycle cultures kinetics of substrate utilization. Appl.
632 Biochem. Biotechnol. 66, 69–81. https://doi.org/10.1007/BF02788808
633 Verduyn, C., Postma, E., Scheffers, W.A., Van Dijken, J.P., 1992. Effect of benzoic acid on metabolic
634 fluxes in yeasts: A continuous-culture study on the regulation of respiration and alcoholic
635 fermentation. Yeast 8, 501–517. https://doi.org/10.1002/yea.320080703
636 Weusthuis, R.A., Adams, H., Scheffers, W.A., van Dijken, J.P., 1993. Energetics and kinetics of maltose
637 transport in Saccharomyces cerevisiae: a continuous culture study. Appl. Environ. Microbiol. 59,
638 3102–3109. https://doi.org/10.1128/aem.59.9.3102-3109.1993
639